PAPER

Check for updates

Investigating naproxen removal from pharmaceutical factory effluents using UVA/MIL-88-A/PS and solar/MIL-88-A/PS systems†

Sarah Ghazali,[a] Abbas Baalbaki, [iD][a] Weam Bou Karroum,[a] Alice Bejjani [iD] *[b] and Antoine Ghauch [iD] *[a]

MIL-88-A, an iron-based metal–organic framework (MOF), was synthesized and investigated for its potential as a mediator in a solar-powered system for the activation of persulfate (PS). Solar/MIL-88-A/PS and UVA/MIL-88-A/PS systems were evaluated for the degradation of naproxen (NAP) in water. Control experiments were conducted to study the activation of PS by MIL-88-A in the absence and presence of either UVA lamps or sunlight. Both systems were optimized and tested for their recyclability and matrix variations by varying water-quality parameters, including pH, salinity, bicarbonates, and phosphates. The results indicated that (i) 87% of NAP ($[NAP]_0$ = 50 mg L^{-1}) was degraded within a period of 100 min in UVA/MIL-88-A/PS system, whereas complete degradation occurred in 10–15 min in solar/MIL-88-A/PS system; (ii) MIL-88-A can be recycled over five cycles for PS activation without any regeneration process; and (iii) carbonates and phosphates have inhibitory effect on the degradation of NAP in both systems. The degradation mechanism was elucidated using EPR, TOF-SIMs, and HPLC-MS, which revealed that the degradation mechanism is based on oxidation by hydroxyl (HRs) and sulfate radicals (SRs). Three NAP degradation products were identified using an HPLC-QTOF high-resolution mass spectrometer.

Environmental significance

Pharmaceutical industries are encountering the challenge of efficiently treating wastewater containing PPCPs. Biological treatment is not effective; therefore, chemical treatments such as Fenton and AOPs, particularly persulfate-based AOPs, have been the treatments of choice. Persulfate treatment is energy intensive, and solarization is not yet a viable option. This study investigated solar powered persulfate treatment using MIL-88-A as an energy mediator.

1. Introduction

The environmental contamination with pharmaceuticals and personal care products (PPCPs) has raised major concerns among scientific and regulatory communities during the last three decades, and a significant number of studies have been conducted to determine the environmental and human health effects of PPCPs present in nature.[1] PPCPs of several categories, including hormones, antibiotics, NSAIDs, and fragrances, among others, have been classified as emerging contaminants owing to their possible hazard to the aquatic environment and human health. Once in the aquatic environment, PPCPs have been found to alter the physiological processes in fish by binding to their nuclear receptors, which modify molecular mechanisms at the transcription and/or translation levels.[2,3] Their increased global occurrence is attributed to the increasing human population and the increase in life expectancy.[4–6] All these factors contribute to an increase in the quantity and variety of pharmaceuticals ingested and subsequently released into the environment. PPCPs can enter the environment through different routes; however, significant quantities are produced from manufacturing facilities and wastewater treatment plants.[7,8] Active pharmaceutical ingredients (APIs) from different PPCPs were found in wastewater treatment plants in quantities ranging from ng L^{-1} to μg L^{-1} (ref. 4) in several countries around the world.[9–13] Conventional wastewater treatment technologies proved to be ineffective for the removal of PPCPs since the compounds are designed to have high chemical stability.[6]

Nonsteroidal anti-inflammatory drugs (NSAIDs), such as naproxen, ibuprofen, and ketoprofen, are a major category of PPCPs.[6] They are frequently used owing to their inexpensive cost, over-the-counter availability, and minor side effects. As

[a]*American University of Beirut, Faculty of Arts and Sciences, Department of Chemistry, P. O. Box 11-0236, Riad El Solh, 1107-2020 Beirut, Lebanon. E-mail: antoine.ghauch@aub.edu.lb; Fax: +961 1 365217; Tel: +961 1 350000*

[b]*Lebanese Atomic Energy Commission, CNRS, Research and Development Department, P. O. Box 11-8281, 1107-2260 Riad EL Solh, Beirut, Lebanon. E-mail: abejjani@cnrs.edu.lb; Fax: +961 1 450810; Tel: +961 1 450811*

† Electronic supplementary information (ESI) available. See DOI: https://doi.org/10.1039/d3va00290j

© 2024 The Author(s). Published by the Royal Society of Chemistry

Environ. Sci.: Adv., 2024, **3**, 119–131 | 119

a result, considerable amounts of NSAIDs and their metabolites enter groundwater and surface and drinking water.[14,15] These products have pK_a values ranging from 4.1–4.9; therefore, they exist as soluble ions at the neutral pH of surface water, causing them to be more resistant to removal.

Advanced oxidation processes (AOPs) have recently acquired an increasing interest in wastewater treatment technologies since they have shown efficiency in the elimination of organic compounds that can be hard to remove by conventional wastewater treatment technologies.[14] AOPs generate reactive species, such as hydroxyl radicals (HRs), which rapidly and non-selectively degrade a wide range of organic pollutants *via* oxidation.[3,9,16] Common AOPs currently used in industrial WWTPs include UV-based processes (UV/H$_2$O$_2$, UV/H$_2$O$_2$/O$_3$, *etc.*), ozonation, Fenton's reaction (Fe^{2+}/H$_2$O$_2$), and, more recently, persulfate-based AOPs (PS-AOPs).[17–19]

PS-AOPs have been increasingly recognized as powerful strategies for the remediation of organic pollutants. These approaches harness persulfates as precursors, which, upon activation, give rise to highly reactive oxidants. Sulfate radicals (SRs) are one of the most potent highly reactive oxidants, possessing an oxidation potential (E_0) of 2.6 V, which allows them to engage in rapid and efficient oxidation reactions with a wide array of organic compounds.[12,13]

Three primary persulfate compounds are employed in PS-AOPs: peroxydisulfate (PDS), peroxymonosulfate (PMS), and sulfite. Each of these precursors has unique chemical characteristics, influencing their activation requirements and the diversity of reactive species they produce:

(1) Peroxydisulfate (PDS) – PDS is a robust oxidizing agent that can be activated thermally, chemically, or using radiation to produce sulfate radicals. The PDS activation energy is relatively high, which necessitates strong initiating conditions but results in the generation of powerful radicals capable of degrading complex organic molecules. PDS is characterized by its affordability, stability, ease of transport/safety, and commercial availability at a mass scale, allowing it to be a better choice compared to competitors such as H$_2$O$_2$ and peroxymonosulfate (PMS).[20,21]
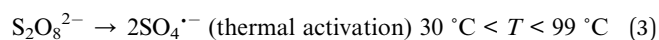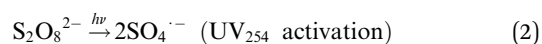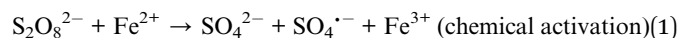
(2) PMS, also known as OXONE®, can be activated under milder conditions compared to PDS. It can generate both sulfate radicals and other reactive species under ambient conditions, offering versatility in treatment applications but causing it to be more reactive and difficult to handle than PDS; additionally, it is more expensive.[20,21]

(3) Sulfite, while less commonly used, distinguishes itself from previously mentioned precursors by generating reductive species such as sulfite radicals, hydrated electrons, and hydrogen radicals upon UV activation and has been effectively used for the removal of several organic and inorganic contaminants.[22]

Non-radical species, such as singlet oxygen (^{1}O$_2$), which can be formed alongside or instead of radicals depending on the activation conditions and the type of persulfate used, also contribute to the pollutant degradation process. Singlet oxygen has considerable oxidizing potential and reacts with

a multitude of organic compounds, further broadening the scope of PS-AOPs in treating complex wastewater streams.[23]

Upon activation, PDS ($E^0 = 2.1$ V) generates sulfate radicals ($E^0 = 2.6$ V).[12,13] This technique is environmentally friendly compared to other chemical processes.[16] Radical species, mainly sulfate radicals (SRs), can be formed in homogeneous systems *via* electron transfer by chemical activation of persulfate (eqn (1)),[24,25] photolysis (UV$_{254 nm}$) (eqn (2)),[26–28] thermolysis (eqn (3)),[29–31] or in heterogeneous systems where chemical activation can be accomplished using zero-valent iron particles, bi-metallics and tri-metallics iron-based systems,[32] MOFs,[33,34] or magnetite.[35,36]

$$S_2O_8^{2-} + Fe^{2+} \rightarrow SO_4^{2-} + SO_4^{\cdot-} + Fe^{3+} \text{ (chemical activation)} \quad (1)$$

$$S_2O_8^{2-} \xrightarrow{hv} 2SO_4^{\cdot-} \text{ (UV}_{254} \text{ activation)} \quad (2)$$

$$S_2O_8^{2-} \rightarrow 2SO_4^{\cdot-} \text{ (thermal activation) } 30 \text{ °C} < T < 99 \text{ °C} \quad (3)$$

Metal–organic frameworks (MOFs)[37–39] are a novel class of porous materials composed of a metal ion or a cluster of metal ions connected to an organic molecule termed the linker. MOFs were considered coordination polymers in early studies, but it was later discovered that the inorganic part possesses a larger dimensionality that can form layers and frameworks, rather than only chains.[40,41] MOFs are characterized by their high surface area (up to 10 000 m^2 g^{-1}) and high porosity (0.99 cm^3 g^{-1} for MIL-88-A).[42,43] These properties allowed their use in a wide range of applications, such as drug delivery,[44,45] magnetism,[46] polymerization,[47] catalysis,[48] and multiple other applications. One of these applications is the elimination of organic contaminants and dyes from wastewater using adsorption.[40] MOFs-containing metals such as iron and cobalt can be used to activate PS, and several studies investigated the use of MOFs as heterogeneous photocatalysts for the removal of hazardous organic contaminants such as dyes and phenol using Fe-MOF-74,[49] methylene blue using MIL-53,[50] and rhodamine B using MIL-100.[51] In our pursuit of greener alternatives for heterogeneous persulfate activation, we have identified metal–organic frameworks (MOFs) as promising candidates, particularly MIL-88-A. This MOF is synthesized *via* a hydrothermal process, which is a more environmentally benign method since it circumvents the need for toxic organic solvents. MIL-88-A comprises iron (Fe) as the metal center and fumaric acid as the organic linker. Both constituents are selected for their relatively low toxicity, minimal environmental footprint, and affordability. Moreover, iron's role in persulfate activation is well-documented and leveraged in MIL-88-A to facilitate the degradation of organic pollutants. The incorporation of fumaric acid not only contributes to the stability and porosity of the MOF structure but also resonates with our commitment to sustainable treatment methodologies. By employing MIL-88-A, we harness the synergistic effect of its components to enhance the activation of persulfate, providing an efficient and eco-friendly approach to wastewater remediation.[52]

In this study, we investigated the total degradation of NAP in UVA/MIL-88-A/PS and solar/MIL-88-A/PS systems and

methodologically assessed the oxidation process efficiency. Furthermore, we assessed the effect of water spectator ions (matrix) on NAP degradation. Finally, we proposed a degradation mechanism of NAP based on the identification of the transformation products of NAP along with the characterization of the MIL-88-A after the reaction using TOF-SIMS.

2. Chemical reagents

Naproxen sodium (NAP) ($C_{14}H_{13}NaO_3$), sodium persulfate (PS) ($Na_2S_2O_8$, purity $\geq 99\%$), phosphate buffer monobasic (H_2NaO_4P assay $\geq 99.0\%$), and dibasic ($HNaO_4P$ assay: 98–100.5%) were purchased from Sigma-Aldrich. Fumaric acid (C_4H_4O) and iron(III) chloride ($FeCl_3$) (both reagent grade >97%) used in the synthesis of MIL-88-A were acquired from Sigma-Aldrich (France and Switzerland, respectively). Ethanol (absolute) was purchased from Scharlau (Spain). Formic acid and acetonitrile used as HPLC mobile phases were acquired from Loba Chemie (India) and Honeywell (Germany), respectively. Millipore deionized water (DI) was used in the preparation of all solutions. To evaluate the matrix effect, sodium bicarbonate ($NaHCO_3$) and sodium chloride ($NaCl$) were acquired from Fluka (Netherlands). Furthermore, hydrochloric acid (HCl) and sodium hydroxide used to adjust the pH were purchased from Fluka (Switzerland and Germany, respectively).

3. Synthesis and characterization methodology of MIL-88-A

MIL-88-A was synthesized using the hydrothermal technique.[36,43,53] This method was selected since it is more environmentally friendly than the conventional solvothermal method. This was performed by adding 1949 mg of fumaric acid and 4544 mg of ferric chloride to a beaker filled with 84 mL of DI. The mixture was stirred for 1 h using a magnetic stirrer at 300 rpm for homogenization. Next, the mixture was transferred to a 100 mL PTFE-lined stainless-steel autoclave bomb, heated at 85 °C for 24 h, and left to cool to room temperature. The solid product was collected and washed with 1 : 1 ethanol and DI in a beaker and left undisturbed for 2 h. Next, the solution containing MIL-88-A suspended crystals was transferred to 50 mL Falcon tubes, and the crystals in each tube were recovered by centrifugation at 4000 rpm ($2200g$) for 10 min. The collected crystals were then washed three times with 390 mL of ethanol/ DI (1 : 1) solution and twice with DI to ensure that all unreacted fumaric acid and ferric chloride were completely removed. Finally, the MOF was dried in a vacuum oven at 85 °C for 24 h and yielded 2350 ± 220 mg of pure MIL-88-A, which was characterized to ensure its purity. Synthesized MIL-88-A characterization methodology was part of a previously conducted research in our laboratory.[33,34]

4. Reaction setup

All experiments were conducted in 110 mL homemade watertight borosilicate tubes that were attached radially to
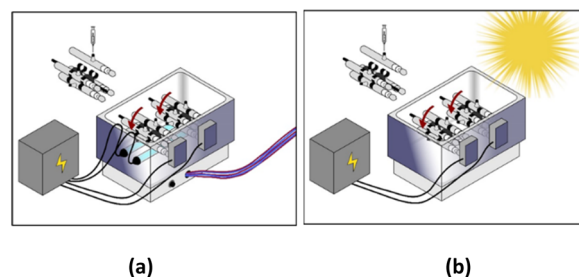

(a)   **(b)**

Fig. 1 Experimental setup of (a) UVA/MIL-88-A/PS/NAP and (b) solar/ MIL-88-A/PS/NAP systems.

a Labquake rotisserie shaker spinning at 8 rpm. All the "stirring" in our experiments was performed using this rotisserie setup. Reactors were placed in a stainless-steel reflector, with two commercial T5 8 watts near-ultraviolet (UVA) fluorescent lamps placed under the reactors (Fig. 1a). The major emission in this spectrum was between 350–450 nm, which is within the UVA-Vis range. Regarding the solar system, UV lamps were removed, and irradiation relied only on direct solar beams without the use of any sunlight concentrator (Fig. 1b). The solar UV (290–390 nm) flux measured at the start and the end of the experiment was equal to 3840 μW cm^{-2} and 3490 μW cm^{-2}, respectively. The solar UV flux was measured using a UV light meter (Lutron UV-340A). This mixing setup was implemented to keep MIL-88-A suspended during irradiation.

5. Experimental conditions and procedures

All solutions were prepared on a daily basis using DI. NAP stock solution (100 mg L^{-1}) was prepared by dissolving 109.5 mg of NAP sodium in a 1000 mL volumetric flask and stirring overnight in the absence of light. PS stock solution (100 mM) was prepared by dissolving 2.381 mg of sodium PS in a 100 mL volumetric flask. Regarding the experiments that were conducted in the presence of UVA, the required volume of NAP stock for the desired concentration was added with the corresponding amount of DI to a 110 mL homemade watertight borosilicate recipient containing the essential amount of MIL-88-A. It was attached radially to a Labquake rotisserie shaker of 8 rpm speed and left to stir for 1 h to reach equilibrium adsorption. The medium was then spiked with the required volume of PS stock solution, where continuous mixing was maintained to ensure solution uniformity. Next, 1.5 mL samples were collected 30 s before and after the addition of MIL-88-A, 30 s after the addition of PS, and every 20 min thereafter for the next 1 h and 40 min. All samples were filtered using 0.45 μm PTFE 13 mm disc filters (Jaytee Biosciences Ltd., UK) and stored in amber-coloured HPLC vials at 4 °C before analysis.

Regarding experiments conducted under solar irradiation, the following changes were performed: the total reaction time was 2 h, the equilibration period of 1 h occurred in the absence of solar radiation in a shaded area, and samples were collected in 5 min intervals for 25 min after spiking with PS and every

© 2024 The Author(s). Published by the Royal Society of Chemistry

Environ. Sci.: Adv., 2024, **3**, 119–131 | **121**

10 min thereafter for the rest of the runtime. Sample collection times were varied based on different experimental requirements. Control experiments were conducted either in the absence of PS and/or MIL-88-A and/or UV. All experiments were performed in triplicates, and each sample was analysed twice for uncertainty determination.

6. Chemical analysis

Quantification of NAP was performed using an HPLC/DAD system (Thermo Ultimate 3000 UHPLC) equipped with a quaternary pump, a vacuum degasser, an autosampler unit maintained at a temperature of 4 °C, and a thermally controlled column compartment set at a temperature of 30 °C. The column used was a C-18 reverse phase column (5 μm; 4.6 mm in internal diameter × 250 mm in length) connected to a security guard column HS C-18 (5 μm; 4.0 mm in internal diameter × 20 mm in length). The detector used was a DAD-3000 (RS) diode-array detector (DAD). The mobile phases consisted of 0.1% (v/v) formic acid (45%) and acetonitrile (55%) under a flow rate of 1 mL min^{-1} and an injection volume of 10 μL, all under isocratic mode. NAP had a retention time of 7.6 min, detected at 228 nm. The linear dynamic range (LDR) obtained was between 0.1–10 mg L^{-1}, with LOD 0.9 μg L^{-1} (Fig. S1†). MS analysis was performed using a high-resolution mass spectrometer detector (HRMS X500R QTOF MS) equipped with a quaternary pump, a vacuum degasser, an auto-sampler with cooling maintained at 4 °C, and a thermally controlled column compartment set at 30 °C. DAD and X500R QTOF MS detectors were used. A reverse-phase C-18 column (100 × 2.1 mm) was used for the elution process. The mobile phase consisted of solvent A (0.1% formic/99.9% methanol) and solvent B (0.1% formic acid/99.9% deionized water), with the following chromatographic elution conditions: 0–16.5 min, gradient 95% to 5% A, 16.5–21.5 min, gradient 95% to 5% B, whereby the flow rate was kept constant at 0.4 mL min^{-1}, and the run time was 25 min.

7. Results and discussion

7.1. Characterization results of the synthesized MIL-88-A

SEM images demonstrated MIL-88-A crystals exhibiting hexagonal rod-like morphology, which is the morphology reported in the literature.[36,54] The rod-like crystals were in the nm scale, with sizes ranging from 100–800 nm, as shown in Fig. 2a. The XRD pattern showed peaks with well-defined edges that were visible at 2θ positions of 7.7°, 10.6°, and 12.9° (Fig. 2b).[36,54] These peaks are consistent with previously reported patterns[48,49] and theoretical simulated ones, demonstrating the crystalline structure of MIL88-A and indicating a successful synthesis. Freshly synthesized MIL-88-A was previously characterized by our research group. MIL-88-A was used in a PS system as a mediator for SMX and NAP degradation.[33,34]

7.2. MIL-88-A/PS system controls

In our study, we explored the performance of the MIL-88-A/PS system under both UVA and solar irradiation to address the
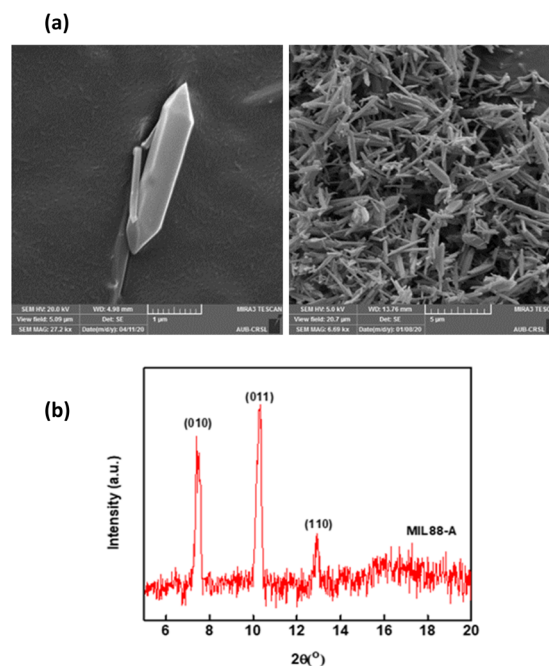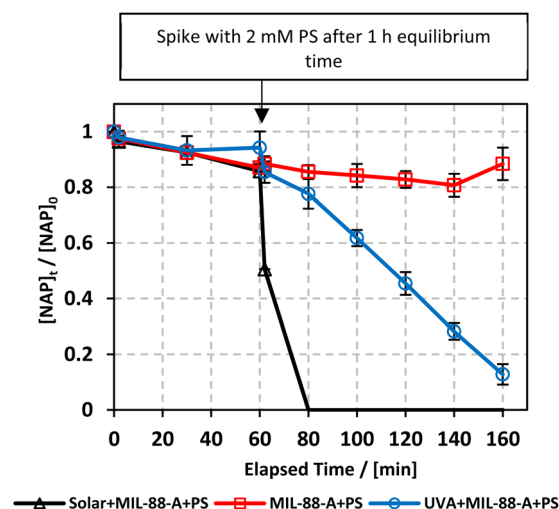

Fig. 2 Characterization of the synthesized MIL-88-A: (a) SEM of MIL-88-A crystals at different magnifications (b) XRD diffraction pattern.

variability in solar availability across different geographical locations. This comparison is crucial for understanding the potential of UVA as a surrogate for natural sunlight in regions with inconsistent or limited solar exposure. Our findings aim to inform the adaptation of photocatalytic technologies to diverse environmental conditions, ensuring their efficiency and applicability, regardless of natural light availability. The MIL-88-A/PS system only achieved 11.6% degradation in 60 min after the PS spike. In the UVA/MIL-88-A/PS and solar/MIL-88-A/PS systems,

Fig. 3 Elimination of NAP in a combined MIL-88-A/PS system and the presence of solar or UVA light. Experimental conditions: [NAP]$_0$ = 50 mg L^{-1}, [PS]$_0$ = 2 mM, [MIL-88-A]$_0$ = 25 mg L^{-1}. Error bars are calculated as $\frac{ts}{\sqrt{n}}$, where absent bars fall within the symbols.

the % degradation increased to 87.2% and 99.8%, respectively, as shown in Fig. 3.

The enhanced photocatalytic performance under solar irradiation can be attributed to the optical properties of MIL-88A. With a band gap of 2.51 eV,[55] MIL-88A is well-aligned with the band gap characteristics (<3 eV) of iron-based metal–organic frameworks (Fe-MOFs), which are conducive to visible-light-driven photocatalysis.[56] This band gap allows MIL-88A to utilize a significant portion of the solar spectrum, specifically the visible range, where it exhibits strong absorbance bands. The absorption profile from the literature-reported DRS analysis reinforces the suitability of MIL-88A for solar-driven applications.[55]

Furthermore, the intensity of light plays a pivotal role in photocatalysis, influencing the generation of charge carriers on the MOF surface. Under solar irradiation, the increased photon flux can promote higher electron generation, thereby mitigating the electron–hole recombination issue, a known limitation in Fe-MOFs.[56] This enhances the activation of persulfate, leading to improved degradation efficiency.

These observations and analyses underscore the relevance of our study's focus on solar irradiation and offer valuable insights for leveraging the photocatalytic capabilities of MIL-88A in various environmental conditions.

7.3. UVA/MIL-88-A/PS system

To study the photochemical degradation process of NAP in the MIL-88-A/PS system, control experiments were performed under UVA irradiation. The UVA/MIL-88-A/PS/NAP setting was compared to two other settings: in the presence of persulfate only (UVA/PS/NAP) and MIL-88-A only (UVA/MIL-88-A/NAP) under the abovementioned conditions. The drop in [NAP] after 60 min was 19.25% and 51.31%, respectively, in the MIL-88-A-only and PS-only systems (Fig. 4). This is mainly due to the low concentration of SRs produced by PS photolysis present in the bulk solution. However, the % degradation increased to 87.2% when MIL-88-A and PS were combined (UVA/MIL-88-/PS system). This demonstrated the role of UVA in catalysing PS activation both at the surface of MIL-88-A and in the bulk solution, as shown in previous research.[33] The observed degradation rate constant (k_{obs}), determined by applying eqn (4) based on the pseudo-first-order kinetics model, where k_{obs} represents the rate constant (min^{-1}), and t represents the elapsed time in minutes, exhibited a strong correlation, as shown in Fig. 4. k_{obs} dropped from 18.43×10^{-3} min^{-1} in the UVA/MIL-88-A/PS system to 6.15×10^{-3} min^{-1} in the UVA/PS system. Fig. S2† shows the by-product chromatogram formed under UVA irradiation in the UVA/MIL-88-A/PS system. The next sections demonstrate an optimization strategy to improve NAP degradation that was guided by these results.

$$\ln[\text{NAP}]/[\text{NAP}]_0 = -k_{obs}t \qquad (4)$$

7.4. Solar/MIL-88-A/PS system

Experiments were performed to study the effectiveness of solar/MIL-88-A/PS on NAP degradation. According to the literature, NAP is photosensitive and demonstrates full degradation after being exposed to sunlight.[57–61] A 100 mL solution containing $[\text{NAP}]_0 = 50$ mg L^{-1} was added to 25 mg L^{-1} of $[\text{MIL-88-A}]_0$, and
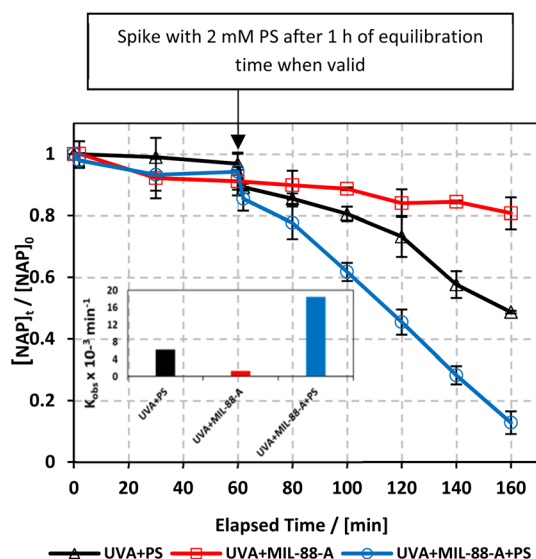

Fig. 4 The % degradation of NAP irradiated with UVA lamps as a function of time (min) in three reactions under different conditions: PS only, MIL-88-A only, and MIL-88-A with PS. Reactors were irradiated by the UVA lamps placed on the side. Experimental conditions: $[\text{NAP}]_0 = 50$ mg L^{-1}, $[\text{PS}]_0 = 2$ mM, $[\text{MIL-88-A}]_0 = 25$ mg L^{-1}. Error bars are calculated as $\frac{ts}{\sqrt{n}}$, where absent bars fall within the symbols. The inset is a plot of k_{obs} for the different studied systems.
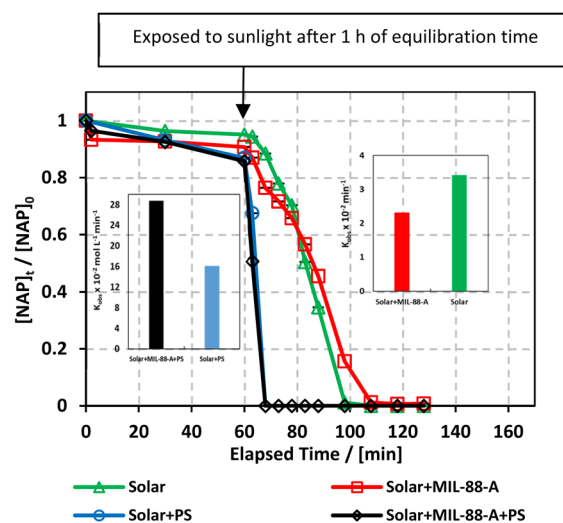

Fig. 5 The % degradation of NAP irradiated with solar energy as a function of time (min) under different conditions: PS only, MIL-88-A only, and MIL-88-A with PS. Reactors were put under sunlight in a rotisserie shaker. Experimental conditions: $[\text{NAP}]_0 = 50$ mg L^{-1}, $[\text{PS}]_0 = 2$ mM, $[\text{MIL-88-A}]_0 = 25$ mg L^{-1}. Error bars are calculated as $\frac{ts}{\sqrt{n}}$, where absent bars fall within the symbols. The insets are plots of k_{obs} of zero-order kinetics (left side) and pseudo-first-order kinetics (right side).

© 2024 The Author(s). Published by the Royal Society of Chemistry

Environ. Sci.: Adv., 2024, **3**, 119–131 | **123**

the solution was left to stir in the dark for 1 h to reach equilibrium adsorption. Next, the medium was spiked with $[PS] = 2$ mM, and continuous stirring was maintained to ensure uniform mixing. Next, the system was placed under sunlight. During the experiments, the solar UV (290–390 nm) reached a maximum of 3900 μW cm^{-2} and decreased to reach 3500 μW cm^{-2} at the end of the reaction. PS and MIL-88-A were separately added to the system to optimize NAP degradation, while also accounting for the impact of each additive on NAP degradation. All control experiments showed 100% degradation of NAP in less than 20 min of reaction time (Fig. 5). However, the results obtained in the combined solar/MIL-88-A/PS system had the added advantage of degrading both NAP and its by-products, as attested by the results shown in Fig. S3 and S4.†[28,29,62] In fact, the time course of NAP by-products showed different kinetics of appearance/disappearance than NAP. The most significant system was the one combining MIL-88-A and PS under solar irradiation, which demonstrated complete removal of the by-products, without the significant resistance observed in the solar and solar/MIL-88-A systems. The investigation of the solar-powered system kinetics provided valuable insights into the underlying mechanisms. The observed rate orders shed light on the reaction dynamics and highlight the role of sunlight in driving these processes. The solar/MIL-88-A/PS system and solar/PS control were found to exhibit zero-order kinetics (eqn (5)), with determined $|k_{obs}|$ values of approximately 28.6×10^{-2} mol L^{-1} min^{-1} and 16.0×10^{-2} mol L^{-1} min^{-1}, respectively. On the other hand, controls involving solar/NAP and solar/MIL-88-A displayed pseudo-first-order kinetics. This suggests that the higher solar radiation intensity provides more energy for the generation of sulfate radicals. These sulfate radicals propagate a radical chain reaction, where they continuously oxidize naproxen. The faster kinetics with solar-based systems (solar/PS and solar/MIL-88-A/PS) is indicated by the complete degradation of NAP and degradation by-products, as tested by HPLC (Fig. S3†), in contrast to the accumulation of the by-products in the other systems. Moreover, one cannot neglect the role of thermal PS activation due to the slight increase of the temperature of the reactors exposed to solar irradiation from room temperature to 40 °C after 120 min of reaction time[57,63] Comparative analysis of our solar/MIL-88-A/PS/NAP system with the literature revealed a marked enhancement in degradation efficiency. Our system exhibits complete degradation of NAP within 20 min, which is notably more efficient than the solar/MIL-88-A/PS/SMX system described by Abou Khalil *et al.*[64] Despite the higher catalyst concentration (125 mg L^{-1}) used in their study, our system achieved full degradation at a lower catalyst loading.

In terms of UVA irradiation, our UVA/MIL-88-A/PS/NAP system attained an 87% degradation rate within 100 min, demonstrating a competitive degradation capability when compared with the reported degradation of SMX under similar conditions.[64] These findings not only underscore the catalytic prowess of MIL-88-A within PS-AOPs but also emphasize the solar-driven system's potential to surpass the performance of systems under artificial UVA irradiation.

While a precise performance comparison is constrained by differences in initial experimental conditions, the presented evidence substantiates the promise of MIL-88-A as a robust catalyst in solar-mediated AOPs for wastewater treatment.

$$[NAP]_t - [NAP]_0 = k_{obs}t \qquad (5)$$

7.4.1. Recyclability. Recyclability is a fundamental parameter when analysing heterogeneous catalysis applications since catalysts that can be recovered and reused are greener and more cost-effective.[65] We conducted an experiment where MIL-88-A was recovered in 5 successive cycles. The recovery process included separation using centrifugation, followed by drying *via* vacuum oven at 90 °C for 24 h. The recovered MIL-88-A quantity decreased after each cycle since some MIL-88-A crystals got stuck in the 0.45 μm PTFE filter used in the sampling process. Therefore, the volume of NAP solution was adjusted for every subsequent cycle such that the concentration of MIL-88-A and NAP remained constant at 25 mg L^{-1} and 50 mg L^{-1}, respectively, to conduct a comparative analysis of the results collected from each cycle. Results showed that a 100% degradation of NAP was obtained in each of the five successive cycles. MIL-88-A catalytic activity increased after each cycle (Fig. 6). The increase in MIL-88-A's catalytic activity over cycles can be linked to the increase in the number of defects present, which in turn increases the number of adsorption sites, as evident from the data displayed in Fig. 5. The first cycle showed around 85% degradation within the first 30 min after spiking with PS compared to the 95% and 98% degradation in cycles 2 and 3, respectively. Additionally, when comparing cycles 3 and 4, MIL-88-A catalytic activity remained constant, whereas NAP degradation rates in both cycles reached 95%. SEM images (Fig. 7a) of MIL-88-A taken after recycling showed that the rod-like morphology of MIL-88-A crystals was identical to that of freshly synthesized MIL-88-A; however, the homogeneity of MIL-88-A crystals was lost when the crystals were extended. The XRD
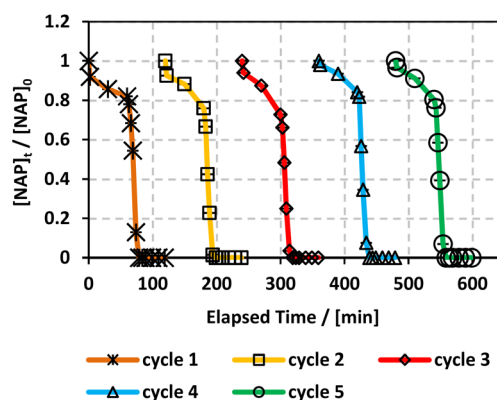

Fig. 6 Recyclability experiments of MIL-88-A in solar/MIL-88-A/PS/NAP system. $[NAP]_0 = 50$ mg L^{-1}, $[PS]_0 = 2$ mM, $[MIL-88-A]_0 = 25$ mg L^{-1}. Error bars are calculated as $\frac{ts}{\sqrt{n}}$, where absent bars fall within the symbols.

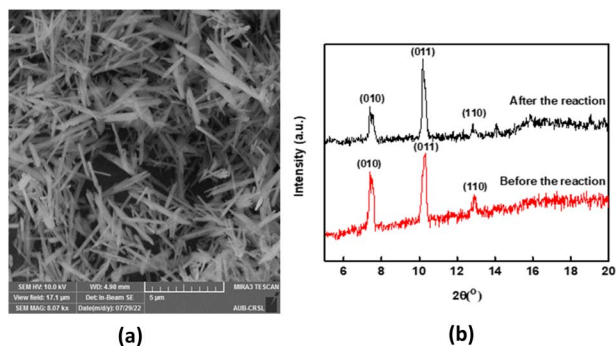**Fig. 7** (a) SEM image of recycled (cycle 1) MIL-88-A (b) XRD pattern of newly *vs.* used MIL-88-A crystals.

Fig. 8 Effect of [NaCl] = 200–20 000 mg L⁻¹ on the degradation of NAP as function of time (min): (a) in the UVA/MIL-88-A/PS/NAP system. The inset is a plot of k_{obs} at different NaCl concentrations and (b) in the solar/MIL-88-A/PS/NAP system. The inset is the degradation by-products profile of NAP under phosphate effect in solar/MIL-88-A/PS at [NaCl] = 20 000 mg L⁻¹. Experimental conditions $[NAP]_0$ = 50 mg L⁻¹, $[PS]_0$ = 2 mM, $[MIL-88-A]_0$ = 25 mg L⁻¹. Error bars are calculated as $\frac{ts}{\sqrt{n}}$ where absent bars fall within the symbols.

diffraction pattern (Fig. 7b) of MIL-88-A is similar to that of the initially synthesized MIL-88-A.

7.5. Matrix effect: solar *vs.* UVA-activated systems

7.5.1. Case of chlorides. The effect of common anions in natural water on NAP degradation was examined in both UVA/MIL-88-A/PS/NAP and solar/MIL-88-A/PS/NAP systems. To mimic salinity in natural water conditions, three different concentrations of chlorides corresponding to freshwater ([NaCl] = 200 mg L⁻¹), brackish water ([NaCl] = 2000 mg L⁻¹), and saline water ([NaCl] = 20 000 mg L⁻¹) were tested.[66] As shown in Fig. 8, the addition of up to 2000 mg L⁻¹ of chlorides in UVA/MIL-88-A/PS/NAP caused a slight inhibition in the % degradation of NAP (overlapped data). A more noticeable inhibition was observed in saline water, as indicated by the decrease in k_{obs} from 14.05×10^{-3} min⁻¹ to 5.30×10^{-3} as the [NaCl] increases from 2000 mg L⁻¹ to 20 000 mg L⁻¹, as seen in Fig. 8a. This is due to the excess of Cl⁻ that would scavenge Cl˙ to produce dichloride radicals, which are less effective than sulfate and/or hydroxyl radicals[67] (eqn (6) and (7)). In the solar/MIL-88-A/PS/NAP system, the addition of chloride ions in the three different concentrations had a less significant effect on NAP degradation but delayed the degradation of all transformation products, as seen in the inset in Fig. 8b. As the concentration of added Cl⁻ increased, the inhibition became more noticeable compared to the NaCl-free system under solar radiation, where NAP and its transformation products underwent full degradation in a much shorter time. These findings are consistent with prior studies on UV/PS activated systems conducted by Ghauch *et al.*[28,29] In these systems, ketoprofen degradation was inhibited in brackish water and, more substantially, in saline water where the concentration of Cl⁻ ions is greater than 10 mM (584 mg L⁻¹ of NaCl), and the chloride quenching effect is more evident. The resistance of the solar/MIL-88-A/PS system to added chlorides can be explained by the generation of Cl˙ having a similar oxidative potential (E_0 = 2.432 V) to sulfate and hydroxyl radicals.[68] pH changes in the experiment were reported in Table S1,† where pH$_i$ decreased from 6.10 to 5.79 and pH$_f$ decreased from 3.73 to 4.56 in the UVA system.
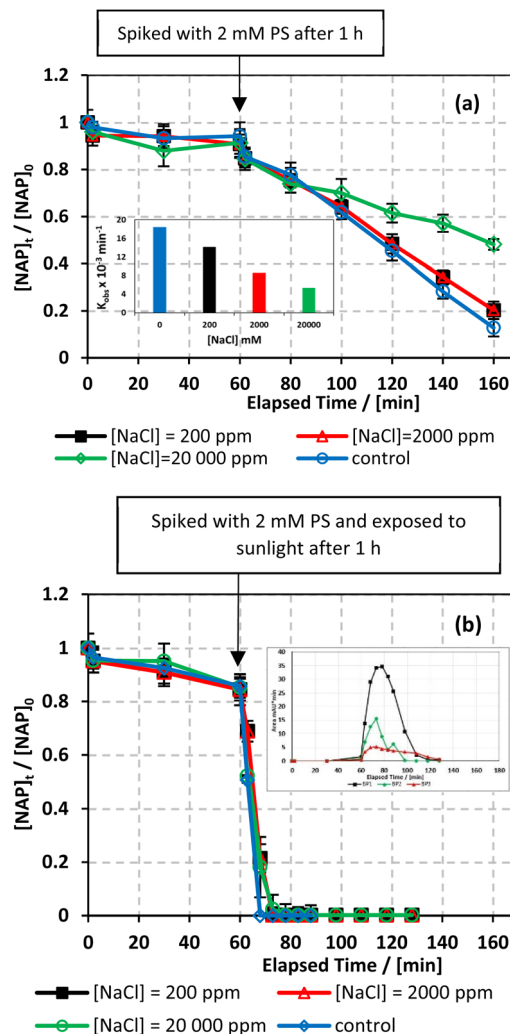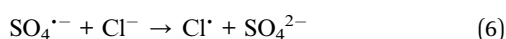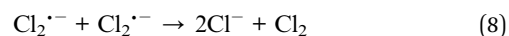
$$SO_4^{\bullet-} + Cl^- \rightarrow Cl^{\bullet} + SO_4^{2-} \qquad (6)$$

$$Cl^{\bullet} + Cl^- \rightarrow Cl_2^{\bullet-} \qquad (7)$$

$$Cl_2^{\bullet-} + Cl_2^{\bullet-} \rightarrow 2Cl^- + Cl_2 \qquad (8)$$

7.5.2. Case of phosphates. The effect of phosphate concentration on the degradation of NAP was investigated in both the UVA/MIL-88-A/PS/NAP and solar/MIL-88-A/PS/NAP systems for two reasons: first, to account for phosphate residues that may elude from conventional wastewater treatment;[69] and second, to study the effect of pH on the degradation of NAP. Therefore, a study on the effect of phosphate buffer (PB) was conducted at three different concentrations of 1, 5, and 10 mM of PB (pH = 4). The results in Fig. 9 show that PB has an inhibitory effect on the degradation process of NAP in both

© 2024 The Author(s). Published by the Royal Society of Chemistry

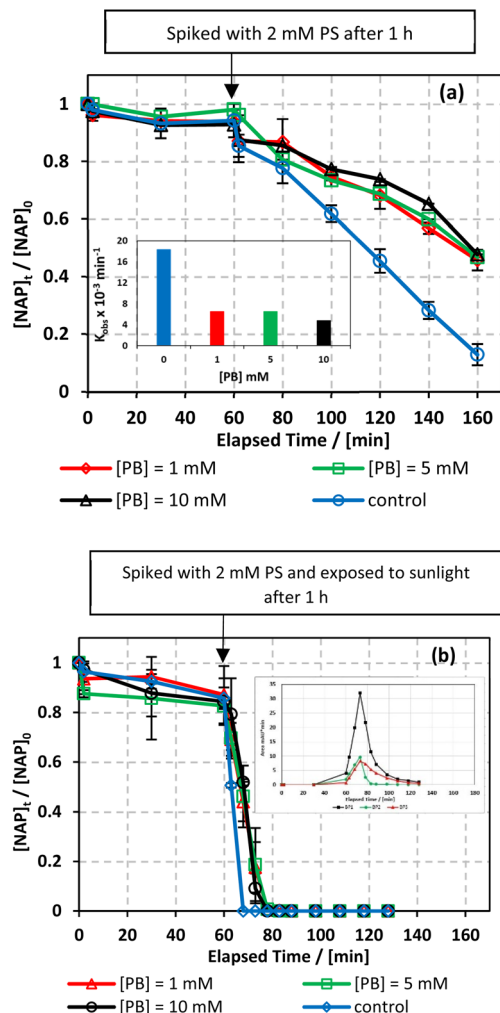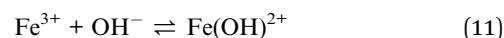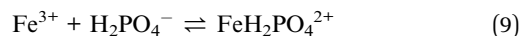*Environ. Sci.: Adv.*, 2024, **3**, 119–131 | 125

Fig. 9 Effect of different phosphate concentrations $[PO_4^{3-}] = 1-10$ mM on the degradation of NAP as function of time (min): (a) in the UVA/MIL-88-A/PS/NAP system. The inset is a plot of k_{obs} at different PO_4^{3-} concentration and (b) in the solar/MIL-88-A/PS/NAP system. The inset is the degradation by-products profile of NAP under phosphate effect in solar/MIL-88-A/PS at $[PO_4^{3-}] = 10$ mM. Experimental conditions $[NAP]_0 = 50$ mg L^{-1}, $[PS]_0 = 2$ mM, $[MIL-88-A]_0 = 25$ mg L^{-1}. Error bars are calculated as $\frac{ts}{\sqrt{n}}$ where absent bars fall within the symbols.

systems. The degradation rate decreased to approximately 50% in the UVA/MIL-88-A/PS/NAP system (Fig. 9a). Notably, k_{obs} decreased from 18.31×10^{-3} min^{-1} in the [PB] free system to 6.53×10^{-3} min^{-1} and 4.74×10^{-3} min^{-1} as [PB] increased from 1 to 10 mM, respectively. However, a full degradation of NAP but not the by-products was observed in the solar/MIL-88-A/PS/NAP system (Fig. 9b), as seen in the insert. This can be explained by the fact that phosphate species form stable complexes with Fe^{2+} ions and accumulate on the surface of MIL-88-A; therefore, free Fe^{2+} ions in solution were adsorbed on the surface of the MOF, preventing the chemical activation of PS. The formation of the iron–phosphate complexes, leading to the production of $FeH_2PO_4^{2+}$ and $FePO_4$, is described below:[70,71]

$$Fe^{3+} + H_2PO_4^- \rightleftharpoons FeH_2PO_4^{2+} \quad (9)$$

$$Fe^{3+} + H_2PO_4^- \rightleftharpoons FePO_4 + 2H^+ \quad (10)$$

$$Fe^{3+} + OH^- \rightleftharpoons Fe(OH)^{2+} \quad (11)$$

$$2Fe^{3+} + 2OH^- \rightleftharpoons Fe_2OH_2^{4+} \quad (12)$$

$$2Fe_2OH_2^{4+} + P(v) \rightleftharpoons Fe_2P^V \quad (13)$$

In our experimental conditions, it is likely that the above-mentioned equations occur, albeit at varying rates. For instance, the hydrolysis reactions of metal cations (Fe^{3+}) (eqn (11)–(13)) would occur rapidly if the solution was devoid of phosphate. However, in the presence of phosphate anions, the hydrolysis reactions are hindered, whereas the formation of the iron–phosphate complex (eqn (9) and (10)) is enhanced. As the reaction progresses, ferric cations are generated concurrently with their complexation with phosphate anions, resulting in the formation of Fe_4P^V, which is a tetranuclear iron–phosphate complex.

This was demonstrated in two independent studies on the degradation of sulfamethoxazole (SMX) and ranitidine (RAN) in Fe/PS systems.[62,72] As shown in Table S1,† both systems showed a decrease in pH_i from 6.10 to 4.66 and from 6.12 to 4.83 in the UVA and solar systems, respectively, as well as an increase in pH_f from 3.73 to 4.25 and from 2.51 to 3.27 in the UVA and solar systems, respectively, when [PB] increased from 1 to 10 mM.

7.5.3. pH effect. A significant factor that affects the degradation of NAP is the pH of the system. The effect of pH on the degradation of NAP in the UVA/MIL-88-A/PS/NAP and solar/MIL-88-A/PS/NAP systems was studied in 10 mM PB solutions with different pH values mimicking acidic, basic, and neutral conditions. The results showed an inhibitory effect in both systems. For example, in the UVA/MIL-88-A/PS/NAP system, the degradation rate decreased to 50% in acidic conditions (pH = 4) and to approximately 25% in neutral and basic conditions (Fig. 10a), where k_{obs} dropped significantly from 18.30×10^{-3} min^{-1} to 2.33, 1.85 and 2.06×10^{-3} at a pH of 4, 7, and 9 respectively. However, in the solar/MIL-88-A/PS/NAP system, a full degradation of NAP but not the by-products was observed, similar to the control system, as seen in the insert (Fig. 10b). In the UVA system, pH_i increased from 6.10 to 8.82, and pH_f increased from 3.73 to 8.41. In the Solar system, pH_i increased from 6.12 to 8.51 and pH_f increased from 2.51 to 7.50, as shown in Table S1.† This may be attributed to the precipitation of non-soluble iron corrosion products on the catalyst's surface, inhibiting the generation of reactive oxidative species (ROS) responsible for the degradation of NAP. As a result, the degradation efficiency was reduced.

7.5.4. Case of bicarbonates. The bicarbonate effect was also examined in both the UVA/MIL-88-A/PS/NAP and solar/MIL-88-A/PS/NAP systems. The presence of bicarbonate caused a noticeable inhibition in the degradation of NAP. In the UVA/MIL-88-A/PS/NAP system, the drop of [NAP] after spiking with PS at $[NaHCO_3] = 1$, 50, and 100 mM decreased from 87.2%, in
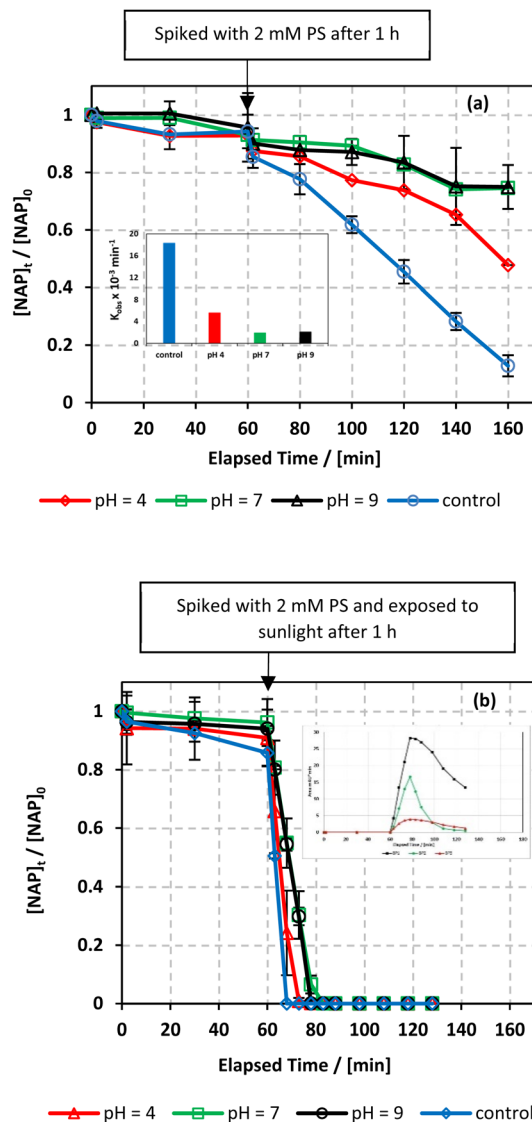
Fig. 10 Effect of pH values on the degradation of NAP as function of time (min): (a) in the UVA/MIL-88-A/PS/NAP system. The inset is a plot of k_{obs} obtained at different pH and (b) in the solar/MIL-88-A/PS/NAP system. The inset is the degradation by-products profile of NAP under pH effect in solar/MIL-88-A/PS at pH = 9. Experimental conditions $[NAP]_0 = 50$ mg L^{-1}, $[PS]_0 = 2$ mM, $[MIL$-88-A$]_0 = 25$ mg L^{-1}. Error bars are calculated as $\frac{ts}{\sqrt{n}}$ where absent bars fall within the symbols.

Fig. 11 Effect of different carbonate concentrations $[CO_3^{2-}] = 1–100$ mM on the degradation of NAP as function of time (min): (a) in the UVA/MIL-88-A/PS/NAP system. The inset is a plot of k_{obs} at different CO_3^{2-} concentrations and (b) in the solar/MIL-88-A/PS/NAP system. The inset is the degradation by-products profile of NAP under carbonate effect in solar/MIL-88-A/PS at $[CO_3^{2-}] = 100$ mM. Experimental conditions $[NAP]_0 = 50$ mg L^{-1}, $[PS]_0 = 2$ mM, $[MIL$-88-A$]_0 = 25$ mg L^{-1}. Error bars are calculated as $\frac{ts}{\sqrt{n}}$ where absent bars fall within the symbols.

the bicarbonate-free system to 28.5%, 21.5%, and 33.3%, respectively (Fig. 11a). k_{obs} decreased by 87.3%, 89.9%, and 81.6% at $[CO_3^{2-}]$ of 1, 50, and 100 mM, respectively. However, in the solar/MIL-88-A/PS/NAP system, a full degradation of NAP but not all by-products was observed, similar to the bicarbonate-free system, as seen in the insert (Fig. 11b). While some previous studies reported an enhancement in the degradation of certain contaminants when HCO_3^- was added,[73–75] the observed inhibitory effect in this study can be attributed to the reaction between HCO_3^- and sulfate radicals (SRs) yielding $CO_3^{\bullet-}$ ($E^0 = 1.59$ V) (eqn (14)), which has moderate oxidative properties towards NAP compared to sulfate radicals.[24] Another reason for the decline in removal efficiency observed could be
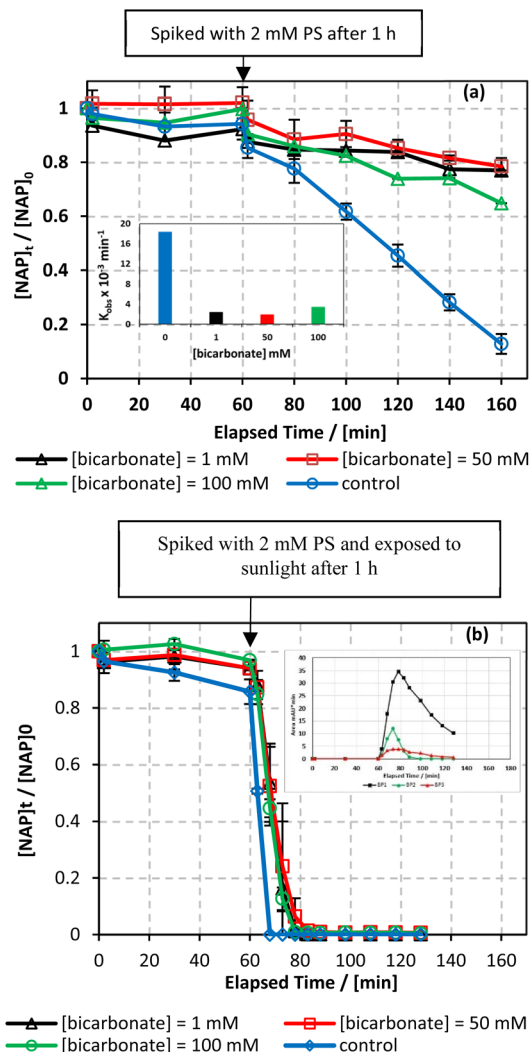
attributed to the adsorption of HCO_3^- onto MIL-88-A, competing with NAP. Zhu *et al.* studied the effect of bicarbonate on a system using α@δ-MnO₂ to activate PMS for the degradation of ciprofloxacin. They found that HCO_3^- can get adsorbed onto the catalyst; therefore, it could obstruct the adsorption and, potentially, the activation mechanism at the surface.[76]

$$SO_4^{\bullet-} + HCO_3^- \rightarrow SO_4^{2-} + CO_3^{\bullet-} + H^+ \qquad (14)$$
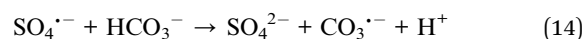
Moreover, the pH_i and pH_f of the solution increased from 6.10 to 8.86 and from 3.37 to 8.59, respectively, as $[HCO_3^-]$

© 2024 The Author(s). Published by the Royal Society of Chemistry

Environ. Sci.: Adv., 2024, **3**, 119–131 | **127**

increased from 0 to 100 mM (Table S1†). A similar inhibition was observed when varying the pH of the system (Section 7.5.3). An earlier study indicated that acidifying a bicarbonate-buffered solution could reverse the inhibitory effect. In fact, acidification removes carbonate species from the solution, favouring the reactivity of SRs with organic pollutants over carbonate species and hydroxyl anions.[24]

7.6. EPR measurements

AOP PS-based systems mainly rely on the formation of SRs and HRs upon activation; however, the identification of these species *via* competitive kinetics using quenchers such as TBA and MeOH may not be very accurate due to strong interferences between quenchers and the active sites of MIL-88-A, the heterogeneous catalyst. As a result, the EPR technique, with common 5,5-dimethyl-1-pyrroline N-oxide (DMPO) as the free radical trapping agent, was chosen as an appropriate analytical technique capable of identifying the presence of radicals to elucidate the role of the expected ROS in the catalytic system of MIL-88-A/PS.[72,77,78]

EPR analysis was used to investigate the presence of radicals in different systems: system 1 (MIL-88-A), system 2 (PS), system 3 (MIL-88-A/PS), and system 4 (MIL-88-A/PS/NAP). The analysis in Fig. S5 and S6† revealed significant peaks in the EPR spectra of systems 2, 3, and 4, indicating the presence of radicals. DMPO–OH adducts suggested the formation of hydroxyl radicals, whereas the presence of DMPO–CH$_3$ adducts indicated the existence of methyl radicals. The results provided insights into the radical reactions occurring in the catalytic systems. Rim *et al.* further discussed the implications of these findings in the context of their study.[33]
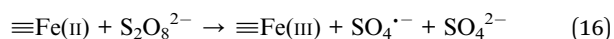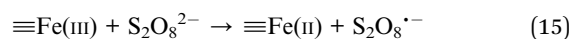
7.7. Degradation mechanism

7.7.1. Identification of degradation products. Three by-products were indicated on HPLC when NAP was degraded in a MOF-activated PS system under the current experimental conditions. The identity of these by-products was further investigated using high-resolution mass spectrometry, as shown in Fig. 12. These by-products have been reported in the literature as well.[79]

7.7.2. Proposed mechanism surface-based activation of PS on MIL-88-A. In our study, the activation of persulfate (PS) under UVA irradiation in the presence of MIL-88-A is postulated to proceed through a radical-driven process. This is corroborated by Electron Paramagnetic Resonance (EPR) data. The MIL-88-A framework harbors Fe(III) centers, originating from the ferric chloride used in its synthesis and serving as active sites for PS activation through a one-electron transfer mechanism.

As depicted in Fig. S7,† the UVA irradiation provides the requisite energy to facilitate the reduction of Fe(III) to Fe(II) within MIL-88-A (eqn (15)). This reduction step is critical for the subsequent cleavage of PS to form sulfate radicals (eqn (16)), which are potent oxidants for degrading NAP molecules.

The overall activation process can be summarized by the following reactions:[33,80,81]

$$\equiv Fe(III) + S_2O_8^{2-} \rightarrow \equiv Fe(II) + S_2O_8^{\bullet-} \tag{15}$$

$$\equiv Fe(II) + S_2O_8^{2-} \rightarrow \equiv Fe(III) + SO_4^{\bullet-} + SO_4^{2-} \tag{16}$$

The dynamic equilibrium between Fe(II) and Fe(III) is crucial since it perpetuates the generation of sulfate radicals. In an aerobic environment, any Fe(II) produced is rapidly reoxidized to Fe(III), thereby sustaining the catalytic cycle and promoting the continuous degradation of NAP molecules.[33,80,81]

Additionally, the presence of H$_2$O within the reaction milieu contributes to the generation of hydroxyl radicals, expanding the diversity of reactive species that target and degrade the NAP.[33,80,81]

This proposed mechanistic pathway aligns with the current literature on radical processes within photochemical AOPs and leverages the intrinsic properties of MIL-88-A to activate PS, without the need for additional chemical reagents or external energy inputs, aside from UVA light. However, it should be noted that the intricate nature of this system prohibits
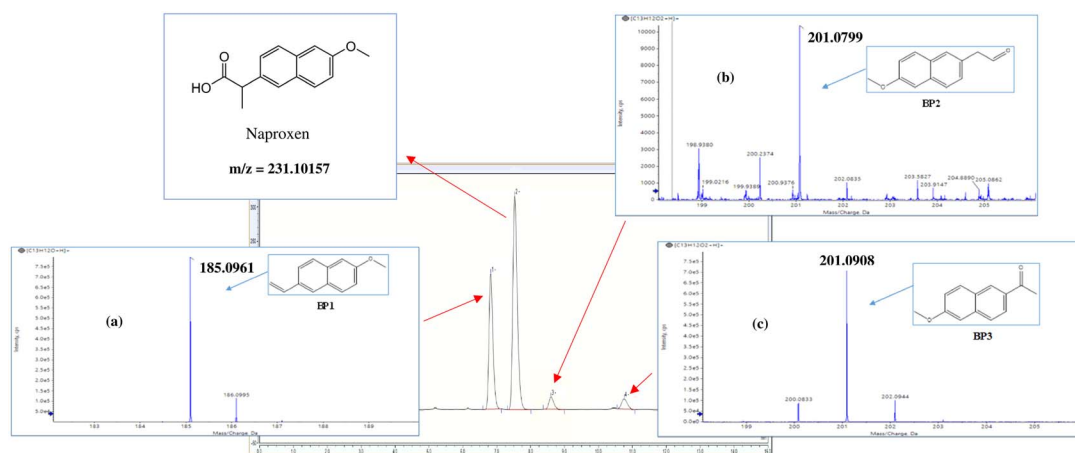

Fig. 12 HPLC chromatogram at $T = 25$ °C showing NAP and its by-products at reaction time $t = 100$ min. Analysis was done on Thermo Ultimate 3000 UHPLC with HR mass spectrum fragmentation pattern of (a) **BP1**, (b) **BP2** and (c) **BP3**.
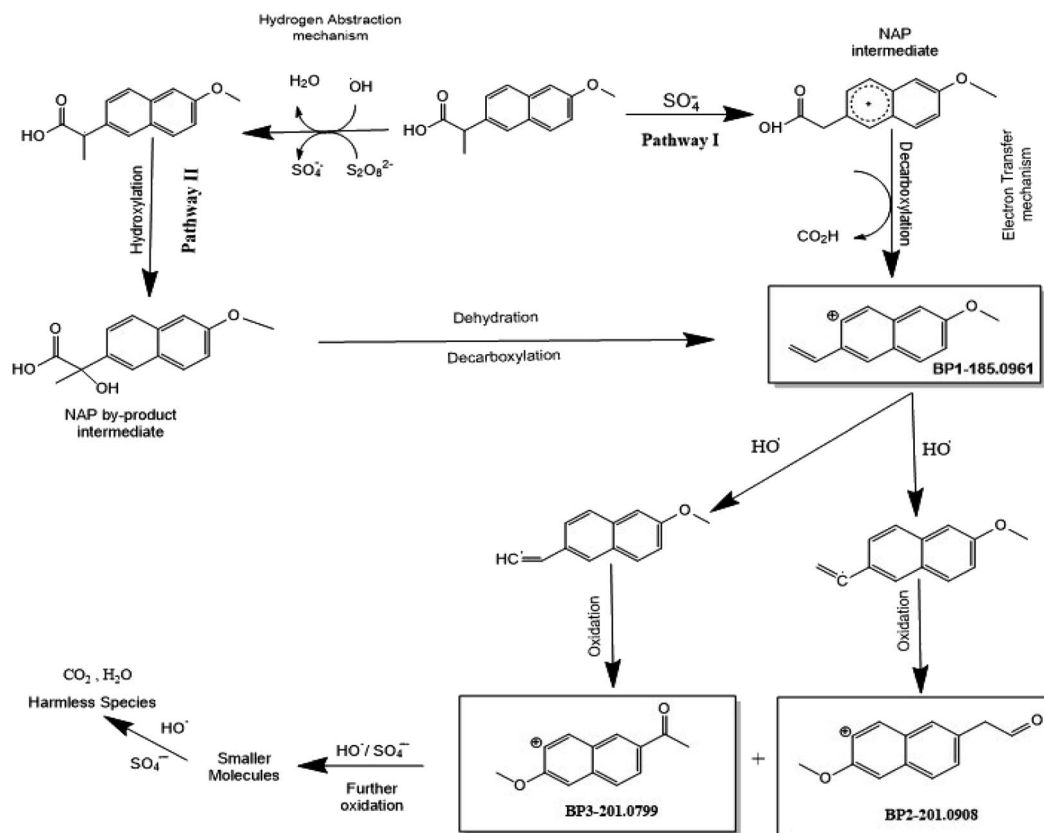
Fig. 13 Overall degradation mechanism of NAP in the UVA/MIL–88–A/PS system.

a straightforward kinetics study using scavengers due to potential secondary interactions with MIL-88-A.

7.7.3. Proposed NAP degradation mechanism. To achieve a better understanding of the NAP degradation mechanism, the TOF-SIMS technique was used, in addition to HPLC/QTOF, to detect and identify NAP degradation products in the UVA/MIL-88-A/PS/NAP and solar/MIL-88-A/PS/NAP systems. The TOF-SIMS technique enables the generation of images of MIL-88-A based on specific atoms or molecular fragments extracted from the overall mass spectrum acquired by the software and from each pixel of the area of interest. The MIL-88-A fiber-like morphology of 3–8 μm length (Fig. S8a†) and the distribution of NAP into the interstices of the fibers (Fig. S8b†) were easily visualized in the collected image of the total positive secondary ion. The green color in Fig. S8b† could be attributed to NAP by-products **BP1** and **BP2** and decarboxylated NAP at 185.0961 m/z. The results clearly showed that adsorption and degradation are the two processes responsible for NAP elimination. Furthermore, accurate mass determination of the obtained by-products with the designed structure was performed to elucidate a plausible degradation mechanism of NAP with two pathways (Fig. 13): Pathway I is the result of NAP decarboxylation upon electron transfer (ET) caused by SRs attack, whereas Pathway II is the result of a decarboxylation/dehydration mechanism occurring after hydroxylation triggered by HRs abstracting hydrogen from NAP. **BP1** ($m/z = 185.0961$) (Fig. 12a) is oxidized in the presence of HRs to form two intermediates, which are

then further oxidized to generate **BP2** ($m/z = 201.0908$) (Fig. 12b) and **BP3** ($m/z = 201.0799$) (Fig. 12c), which are further degraded into undetectable fragments of organic molecules.

8. Conclusion

In this study, NAP was efficiently degraded in a PS-based AOPs system. MIL-88-A, an iron-based MOF synthesized in a green environment, was employed to improve previous findings. NAP degradation systems using two different energy sources (UVA and solar irradiation) were compared. Both UVA/MIL-88-A/PS and solar/MIL-88-A/PS were effective for the removal of NAP in a reasonable amount of time, with solar/MIL-88-A/PS system achieving total degradation of NAP ([NAP] = 50 mg L^{-1}) in just 10–15 min after spiking with PS. Furthermore, only the solar/MIL-88-A/PS quickly achieved the additional degradation of the transformation products, whereas both the solar/MIL-88-A and solar/PS systems did not. This proves the existence of a synergistic effect of all the components of the system that enhances the performance and achieves further mineralization. Our results also showed that MIL-88-A is recyclable and effective over five cycles in PS activation, without the need for any regeneration process. Therefore, we propose MIL-88-A as a potential mediator for solar PS activation in the treatment of hazardous effluents containing pharmaceuticals and difficult-to-degrade organic micro-contaminants. Furthermore, the identification of both zero-order and first-order kinetics

highlights the influence of different factors on the reaction rates. These findings indicate the diverse mechanisms and factors influencing the photochemical reactions of NAP and provide valuable insights for optimizing reaction conditions and understanding the underlying processes. This technology can be applied in facilities where solar is the only available source of energy for large-scale remediation, such as *in situ* chemical oxidation (ISCO). Further research is required to investigate activation using concentrated solar power and to modify MIL-88-A using additional functional groups to enhance catalytic efficiency. Furthermore, other PS activation techniques, such as thermal, ultrasonic, and chemical, should be investigated.

Conflicts of interest

There are no conflicts to declare.

Acknowledgements

References

1 A. B. A. Boxall, M. A. Rudd, B. W. Brooks, D. J. Caldwell, K. Choi, S. Hickmann, E. Innes, K. Ostapyk, J. P. Staveley, T. Verslycke, G. T. Ankley, K. F. Beazley, S. E. Belanger, J. P. Berninger, P. Carriquiriborde, A. Coors, P. C. DeLeo, S. D. Dyer, J. F. Ericson, F. Gagné, J. P. Giesy, T. Gouin, L. Hallstrom, M. V. Karlsson, D. G. Joakim Larsson, J. M. Lazorchak, F. Mastrocco, A. McLaughlin, M. E. McMaster, R. D. Meyerhoff, R. Moore, J. L. Parrott, J. R. Snape, R. Murray-Smith, M. R. Servos, P. K. Sibley, J. O. Straub, N. D. Szabo, E. Topp, G. R. Tetreault, V. L. Trudeau and G. Van Der Kraak, *Environ. Health Perspect.*, 2012, **120**, 1221–1229.

2 V. Burkina, V. Zlabek and G. Zamaratskaia, *Environ. Toxicol. Pharmacol.*, 2015, **40**, 430–444.

3 U. Memmert, A. Peither, R. Burri, K. Weber, T. Schmidt, J. P. Sumpter and A. Hartmann, *Environ. Toxicol. Chem.*, 2013, **32**, 442–452.

4 A. J. Ebele, M. Abou-Elwafa Abdallah and S. Harrad, *Emerging Contam.*, 2017, **3**, 1–16.

5 J. L. Liu and M. H. Wong, *Environ. Int.*, 2013, **59**, 208–224.

6 J. L. Tambosi, L. Y. Yamanaka, H. J. José, R. De Fátima Peralta Muniz Moreira and H. F. Schröder, *Quim. Nova*, 2010, **33**(2), 411–420.

7 P. Bottoni, S. Caroli and A. B. Caracciolo, *Toxicol. Environ. Chem.*, 2010, **92**, 549–565.

8 K. E. Arnold, A. R. Brown, A. R. Brown, G. T. Ankley and J. P. Sumpter, *Philos. Trans. R. Soc., B*, 2014, **369**(1656), DOI: 10.1098/rstb.2013.0569.

9 G. R. Boyd, J. M. Palmeri, S. Zhang and D. A. Grimm, *Sci. Total Environ.*, 2004, **333**, 137–148.

10 D. Ashton, M. Hilton and K. V. Thomas, *Sci. Total Environ.*, 2004, **333**, 167–184.

11 N. Lindqvist, T. Tuhkanen and L. Kronberg, *Water Res.*, 2005, **39**, 2219–2228.

12 N. Nakada, T. Tanishima, H. Shinohara, K. Kiri and H. Takada, *Water Res.*, 2006, **40**, 3297–3303.

13 M. Carballa, F. Omil, J. M. Lema, M. Llompart, C. García-Jares, I. Rodríguez, M. Gómez and T. Ternes, *Water Res.*, 2004, **38**, 2918–2926.

14 R. Andreozzi, V. Caprio, A. Insola and R. Marotta, *Catal. Today*, 1999, **53**, 51–59.

15 P. R. Gogate and A. B. Pandit, *Adv. Environ. Res.*, 2004, **8**, 501–551.

16 N. Lindqvist, T. Tuhkanen and L. Kronberg, *Water Res.*, 2005, **39**, 2219–2228.

17 C. Wei, F. Zhang, Y. Hu, C. Feng and H. Wu, *Rev. Chem. Eng.*, 2017, **33**, 49–89.

18 S. O. Ganiyu, M. Zhou and C. A. Martínez-Huitle, *Appl. Catal., B*, 2018, **235**, 103–129.

19 B. A. Wols and C. H. M. Hofman-Caris, *Water Res.*, 2012, **46**, 2815–2827.

20 J. Wang and S. Wang, *Chem. Eng. J.*, 2018, **334**, 1502–1517.

21 J. Xie, C. Yang, X. Li, S. Wu and Y. Lin, *Chemosphere*, 2023, **339**, 139659.

22 S. Wu, L. Shen, Y. Lin, K. Yin and C. Yang, *Chem. Eng. J.*, 2021, **414**, 128872.

23 Y. Wang, Y. Lin, S. He, S. Wu and C. Yang, *J. Hazard. Mater.*, 2024, **461**, 132538.

24 A. Ghauch, G. Ayoub and S. Naim, *Chem. Eng. J.*, 2013, **228**, 1168–1181.

25 S. Naim and A. Ghauch, *Chem. Eng. J.*, 2016, **288**, 276–288.

26 M. Amasha, A. Baalbaki, S. Al Hakim and R. El Asmar, *J. Adv. Oxid. Technol.*, 2018, **21**(1), 261–273.

27 Y. Liu, X. He, Y. Fu and D. D. Dionysiou, *J. Hazard. Mater.*, 2016, **305**, 229–239.

28 A. Ghauch, A. Baalbaki, M. Amasha, R. El Asmar and O. Tantawi, *Chem. Eng. J.*, 2017, **317**, 1012–1025.

29 M. Amasha, A. Baalbaki and A. Ghauch, *Chem. Eng. J.*, 2018, **350**, 395–410.

30 A. Ghauch, A. M. Tuqan and N. Kibbi, *Chem. Eng. J.*, 2012, **197**, 483–492.

31 A. Ghauch, A. M. Tuqan, N. Kibbi and S. Geryes, *Chem. Eng. J.*, 2012, **213**, 259–271.

32 G. Ayoub and A. Ghauch, *Chem. Eng. J.*, 2014, **256**, 280–292.

33 R. El Asmar, A. Baalbaki, Z. Abou Khalil, S. Naim, A. Bejjani and A. Ghauch, *Chem. Eng. J.*, 2021, **405**, 126701.

34 Z. A. Khalil, A. Baalbaki, A. Bejjani and A. Ghauch, *Environ. Sci. Adv.*, 2022, **1**, 797–813.

35 M. G. Antoniou, A. A. de la Cruz and D. D. Dionysiou, *Appl. Catal., B*, 2010, **96**, 290–298.

36 K. Y. Andrew Lin, H. A. Chang and C. J. Hsu, *RSC Adv.*, 2015, **5**, 32520–32530.

37 S. Wu, Z. Yang, Z. Zhou, X. Li, Y. Lin, J. J. Cheng and C. Yang, *J. Hazard. Mater.*, 2023, **459**, 132133.

38 S. Wu, C. Yang, Y. Lin and J. J. Cheng, *J. Environ. Sci.*, 2022, **115**, 330–340.

39 S. Wu, H. Liu, C. Yang, X. Li, Y. Lin, K. Yin, J. Sun, Q. Teng, C. Du and Y. Zhong, *Chem. Eng. J.*, 2020, **392**, 123683.

40 N. A. Khan, Z. Hasan and S. H. Jhung, *J. Hazard. Mater.*, 2013, **244–245**, 444–456.

41 G. Férey, *Chem. Soc. Rev.*, 2008, **37**, 191–214.

42 P. Z. Moghadam, A. Li, S. B. Wiggin, A. Tao, A. G. P. Maloney, P. A. Wood, S. C. Ward and D. Fairen-Jimenez, *Chem. Mater.*, 2017, **29**, 2618–2625.

43 J. Wang, J. Wan, Y. Ma, Y. Wang, M. Pu and Z. Guan, *RSC Adv.*, 2016, **6**, 112502–112511.

44 P. Horcajada, R. Gref, T. Baati, P. K. Allan, G. Maurin, P. Couvreur, G. Férey, R. E. Morris and C. Serre, *Chem. Rev.*, 2012, 1232–1268.

45 A. C. McKinlay, R. E. Morris, P. Horcajada, G. Férey, R. Gref, P. Couvreur and C. Serre, *Angew. Chem., Int. Ed.*, 2010, **49**, 6260–6266.

46 M. Kurmoo, *Chem. Soc. Rev.*, 2009, **38**(5), 1353–1379.

47 T. Uemura, N. Yanai and S. Kitagawa, *Chem. Soc. Rev.*, 2009, **38**(5), 1228–1236.

48 J. Lee, O. K. Farha, J. Roberts, K. A. Scheidt, S. T. Nguyen and J. T. Hupp, *Chem. Soc. Rev.*, 2009, **38**(5), 1450–1459.

49 S. Bhattacharjee, J. S. Choi, S. T. Yang, S. B. Choi, J. Kim and W. S. Ann, *J. Nanosci. Nanotechnol.*, 2010, **10**, 135–141.

50 J. J. Du, Y. P. Yuan, J. X. Sun, F. M. Peng, X. Jiang, L. G. Qiu, A. J. Xie, Y. H. Shen and J. F. Zhu, *J. Hazard. Mater.*, 2011, **190**, 945–951.

51 H. Liu, X. Ren and L. Chen, *J. Ind. Eng. Chem.*, 2016, **34**, 278–285.

52 X. Li, W. Guo, Z. Liu, R. Wang and H. Liu, *Appl. Surf. Sci.*, 2016, **369**, 130–136.

53 T. Chalati, P. Horcajada, R. Gref, P. Couvreur and C. Serre, *J. Mater. Chem.*, 2011, **21**, 2220–2227.

54 J. Wang, J. Wan, Y. Ma, Y. Wang, M. Pu and Z. Guan, *RSC Adv.*, 2016, **6**, 112502–112511.

55 W. Huang, C. Jing, X. Zhang, M. Tang, L. Tang, M. Wu and N. Liu, *Chem. Eng. J.*, 2018, **349**, 603–612.

56 C. Du, Y. Zhang, Z. Zhang, L. Zhou, G. Yu, X. Wen, T. Chi, G. Wang, Y. Su, F. Deng, Y. Lv and H. Zhu, *Chem. Eng. J.*, 2022, **431**, 133932.

57 A. Baalbaki, G. M. Ayoub, M. Al-Hindi and A. Ghauch, *Sci. Total Environ.*, 2017, **574**, 583–593.

58 Y. He and I. Hua, *Abstracts of Papers of the American Chemical Society*, 2013, vol. 246.

59 J. L. Packer, J. J. Werner, D. E. Latch, K. McNeill and W. A. Arnold, *Aquat. Sci.*, 2003, **65**, 342–351.

60 V. M. Vulava, W. C. Cory, V. L. Murphey and C. Z. Ulmer, *Sci. Total Environ.*, 2016, **565**, 1063–1070.

61 L. Malaeb, G. M. Ayoub, M. Al-Hindi, L. Dahdah, A. Baalbaki and A. Ghauch, *Energy Procedia*, 2017, **119**, 723–732.

62 S. Naim and A. Ghauch, *Chem. Eng. J.*, 2016, **288**, 276–288.

63 S. Al Hakim, A. Baalbaki, O. Tantawi and A. Ghauch, *RSC Adv.*, 2019, **9**, 33472–33485.

64 R. El Asmar, A. Baalbaki, Z. Abou Khalil, S. Naim, A. Bejjani and A. Ghauch, *Chem. Eng. J.*, 2021, **405**, 126701.

65 W. Ren, J. Gao, C. Lei, Y. Xie, Y. Cai, Q. Ni and J. Yao, *Chem. Eng. J.*, 2018, **349**, 766–774.

66 H. A. Gorrell, *Am. Assoc. Pet. Geol. Bull.*, 1958, **42**(10), 2513.

67 D. T. Oyekunle, J. Cai, E. A. Gendy and Z. Chen, *Chemosphere*, 2021, **280**, 130949.

68 Z. Liu, H. Lan, Y. Wang, J. Zhang, J. Qin, R. Zhang and N. Dong, *Chem. Eng. J.*, 2022, **429**, 132485.

69 L. Zhao, Y. Ji, D. Kong, J. Lu, Q. Zhou and X. Yin, *Chem. Eng. J.*, 2016, **303**, 458–466.

70 A. Ghauch, *Chemosphere*, 2008, **71**, 816–826.

71 G. Lente, M. Elizabeth, A. Magalhães and I. Fábián, *Inorg. Chem.*, 2000, **39**, 1950–1954.

72 X. Duan, C. Su, J. Miao, Y. Zhong, Z. Shao, S. Wang and H. Sun, *Appl. Catal., B*, 2018, **220**, 626–634.

73 A. Cai, J. Deng, X. Ling, C. Ye, H. Sun, Y. Deng, S. Zhou and X. Li, *Water Res.*, 2022, **215**, 118288.

74 C. Tan, N. Gao, S. Zhou, Y. Xiao and Z. Zhuang, *Chem. Eng. J.*, 2014, **253**, 229–236.

75 Y. qiong Gao, N. yun Gao, D. qiang Yin, F. xiang Tian and Q. feng Zheng, *Chemosphere*, 2018, **201**, 50–58.

76 S. Zhu, H. Li, L. Wang, Z. Cai, Q. Wang, S. Shen, X. Li and J. Deng, *Chem. Eng. J.*, 2023, **458**, 141415.

77 Y. Liu, X. Chen, Y. Yang, Y. Feng, D. Wu and S. Mao, *Chem. Eng. J.*, 2019, **358**, 408–418.

78 Z. Wei, F. A. Villamena and L. K. Weavers, *Environ. Sci. Technol.*, 2017, **51**, 3410–3417.

79 A. Ghauch, A. M. Tuqan and N. Kibbi, *Chem. Eng. J.*, 2015, **279**, 861–873.

80 K.-Y. A. Lin, H.-A. Chang and C.-J. Hsu, *RSC Adv.*, 2015, **5**, 32520–32530.

81 H. Liu, T. A. Bruton, F. M. Doyle and D. L. Sedlak, *Environ. Sci. Technol.*, 2014, **48**(17), 10330–10336.

© 2024 The Author(s). Published by the Royal Society of Chemistry

Environ. Sci.: Adv., 2024, **3**, 119–131 | **131**